Desalination and Water Treatment
www.deswater.com

doi: 10.1080/19443994.2016.1141375

57 (2016) 23546–23555
October

Taylor & Francis
Taylor & Francis Group

Preparation and properties of iPP hollow fiber membranes for air gap membrane distillation

Juan Wang[a,b,c], Qingfeng He[a,b,c], Yajing Zhao[a,b,c], Pingli Li[a,b,c,*], Heying Chang[a,b,c]

[a]*School of Chemical Engineering and Technology, Tianjin University, Tianjin 300072, P.R. China, Tel. +86 022 27405902; Fax: +86 022 27404347; emails: 15222155772@163.com (J. Wang), 15122687739@163.com (Q. He), chm.gold@163.com (Y. Zhao), tdlpl@163.com (P. Li), changheying@tju.edu.com (H. Chang)*

[b]*Collaborative Innovation Center of Chemical Science and Engineering (Tianjin), Tianjin University, Tianjin 300072, P.R. China*

[c]*Tianjin Key Laboratory of Membrane Science and Desalination Technology, Tianjin University, Tianjin 300072, P.R. China*

Received 26 June 2015; Accepted 28 December 2015

ABSTRACT

Three different thickness isotactic polypropylene (iPP) hollow fiber membranes were prepared for air gap membrane distillation (AGMD) via thermally induced phase separation (TIPS) with cosolvent di-n-butyl phthalate and dioctyl phthalate. A study was carried out to investigate the effect of membrane thickness on the water flux and mechanical properties of the membranes. The ratio of membrane thickness to membrane inner diameter was constant at 0.2. Three relevant AGMD modules were fabricated. During AGMD of 6 wt% salt solution, the influence of inlet temperature of cold brine feed (T_1), membrane thickness on permeate water flux (J_D), gained output ratio (GOR), and thermal efficiency (TE) was experimentally investigated. The maximum J_D could reach 6.62 kg/m^2 h and the maximum GOR could reach 6.95, respectively. Furthermore, the maximum TE was 89.42% which was much higher than that of traditional membrane distillation modules. The results demonstrated that the prepared iPP hollow fiber membrane by TIPS method would be of great potential to be utilized in AGMD process for desalination.

Keywords: Membrane preparation; Isotactic polypropylene; Thermally induced phase separation; Air gap membrane distillation

1. Introduction

Drinkable water scarcity has been a serious problem in recent years because of global population increase and industrial development. Since there are sufficient seawater resources on the earth, desalination emerges as a promising technology to obtain drinkable water [1]. Reverse osmosis as a conventional method to obtain potable water from saline water has complex pre- and post-treatment. Multi-stage flash evaporation needs high temperature and high operation pressure [2]. Membrane distillation (MD), a thermally driven separation process, has been extensively researched for the past three decades [3]. Compared with the conventional desalination process, the potential advantage of MD is that it has the simplicity in operation and low energy consumption because of operating at low temperature and pressure with high salt rejection [4]. Hence MD, a promising technology for desalting saline water, can be regarded as an alternative method for the conventional desalination [5]. MD can be

*Corresponding author.

classified into four configurations including direct contact membrane distillation (DCMD), sweeping gas membrane distillation (SGMD), air gap membrane distillation (AGMD), and vacuum membrane distillation (VMD) [6]. DCMD has the simplest membrane module and is widely applied in MD process. The main drawback of DCMD is its low thermal efficiency (TE) because of the large heat loss by conduction [7]. SGMD has high mass transfer rate and low heat loss because of the non-stationary gas barrier. The main disadvantages of SGMD are its high investment in equipment and high operation cost [8]. VMD can neglect the heat loss and have high permeate flux. However, the membrane during VMD process easily becomes wet [9]. Among the above four different MD configurations, AGMD has more extensive application potential since it presents a stagnant air gap which considerably reduces the heat loss by conduction and the temperature polarization [10].

Although the microporous membrane just plays as a physical barrier, it is decisive during MD process. The membrane which is designed for MD process should be hydrophobic because hydrophobicity can prevent the liquid from entering into its dry pores until the operating pressure exceeds the liquid entry pressure of water (LEPw) [11]. In addition, other membrane characteristics like membrane thickness, pore size, and porosity can also influence the performance of membrane [12–14]. The membrane is in direct contact with the hot brine feed, so membrane with a desirable chemical resistance and thermal stability is suitable for the MD process [4].

The most common materials prepared for membrane are polyvinylidene fluoride (PVDF), polutetrafluoroethylene (PTFE), and polypropylene (PP) [15]. The various ways to prepare hydrophobic membrane are relied on the properties of the polymers. PVDF membrane is prepared by non-solvent induced phase separation (NIPS). The membrane of PTFE can be formed by thermal stretching and heating process. The PP hollow fiber membrane is prepared by melt spinning and cold stretching (MSCS) or thermally induced phase separation (TIPS) [16]. PTFE has the strongest hydrophobicity, oxidation resistance, and thermal stability. But its thermal conductivity is the biggest which leads to the most heat loss and lowest TE. What's more, the preparation of the PTFE hollow fiber membrane is very difficult. PVDF has excellent hydrophobicity, thermal stability, and mechanical strength. Compared with PTFE and PVDF, PP membrane has the advantages of low price and easy preparation. So it has wide market potential [17].

Membrane thickness plays an important role in the resistance to mass transfer. To obtain a high J_D, the membrane should be as thin as possible. On the other hand, in order to achieve high TE, the membrane should be as thick as possible because heat loss by conduction occurs through the membrane matrix in MD process [18–22]. So the membrane thickness should have an optimum thickness. The interest of us is to investigate the influence of membrane thickness on J_D, gained output ratio (GOR) and TE.

Our AGMD module (Fig. 1) was designed to improve the TE because of recycling the latent heat released when the water vapor condensed on the surface of the heat exchange hollow fiber tubes. The latent heat recovered was used to preheat the cold brine feed, which could decrease the heat provided from outside. Therefore, the TE increased [23–26]. The objective in this paper is to prepare isotactic polypropylene (iPP) hollow fiber membranes with different thickness and use them in AGMD process to investigate the influence on J_D, GOR, and the TE. The influence of operation parameter T_1 was also researched. The saline water used in AGMD process is 6 wt%.

2. Experimental

2.1. Materials

iPP (F401, MI = 1.78) was purchased from Daqing Petroleum Chemical (China). Di-n-butyl phthalate (DBP) (analysis grade), dioctyl phthalate (DOP) (analysis grade), and absolute ethyl ethanol were obtained from Tianjin Bodi Chemical Reagents (China). The concentration of DOP and DBP was not less than 99.0 and 99.5%, respectively. All materials were used without further purification.

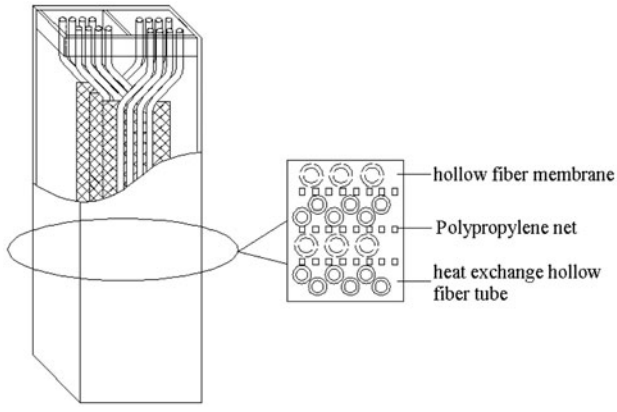

Fig. 1. Schematic presentation of AGMD module.

2.2. Preparation of iPP hollow fiber membranes

iPP hollow fiber membranes were prepared by a batch-type extrusion apparatus which was shown in Fig. 2. The spinneret structure was also shown in Fig. 2. The outer diameter and inner diameter were 0.6 and 0.4 cm, respectively. The iPP particles were dried at 100℃ in oven to remove residual water. Desired amounts of iPP, DBP, and DOP were weighed and poured into a stainless steel vessel. The cell was purged with nitrogen three times to clean the air in it. The nitrogen pressure in the cell increased to 0.2 MPa, then the mixture was subjected to stirring at 210℃ for about 6 h until the mixed iPP/diluents system became a homogeneous melted solution. After the stirrer was stopped, the homogeneous melted solution was degassed under vacuum for half an hour to remove gas bubbles. Then, the homogeneous solution was fed into the spinneret under the nitrogen pressure of 0.2 MPa. The nitrogen was also used as a bore fluid to obtain the hollow fiber membrane. The hollow fiber was extruded from the spinneret, moved through the air, entered into the water quencher to induce phase separation and wound on a take-up winder. The diluents in the membrane were extracted by immersing in absolute ethyl ethanol for 24 h. The final membrane was dried at room temperature for about 3 h.

2.3. Characterization of the hollow fiber membrane

2.3.1. Scanning electron microscopy

The morphology of membrane was observed by a PHILIPS XL30 scanning electron microscope (SEM). Membrane samples were frozen in liquid nitrogen, fractured to obtain fragments, and sputtered with gold.

2.3.2. Pure water flux

PWF of the pre-wet membrane by 95% ethanol solution was measured with a stainless cell at 0.1 MPa pressure and constant feed. Time began to record after 15 min running. The value of pure water flux (PWF) on the basis of the inner surface area of the hollow fiber membrane was the average of five groups.

2.3.3. Tensile break strength measurement

The tensile strength and elongation-at-break of the membrane were determined at room temperature using a WD-10D electronic single yarn tensile tester (Changchun, China) [27,28]. Both ends of the sample were clamped and then the sample was pulled with the tensile rate of 100 mm/min. For each specimen, five runs were performed.

2.3.4. Porosity and mean pore size

The membrane porosity (ε) was defined as the pores volume divided by the total volume of the porous membrane. It could be determined by gravimetric method. Each specimen had five experiments.

The mean pore size of iPP membrane was measured by a porometer (Coulter porometer II), as reported by Yang et al. [29].

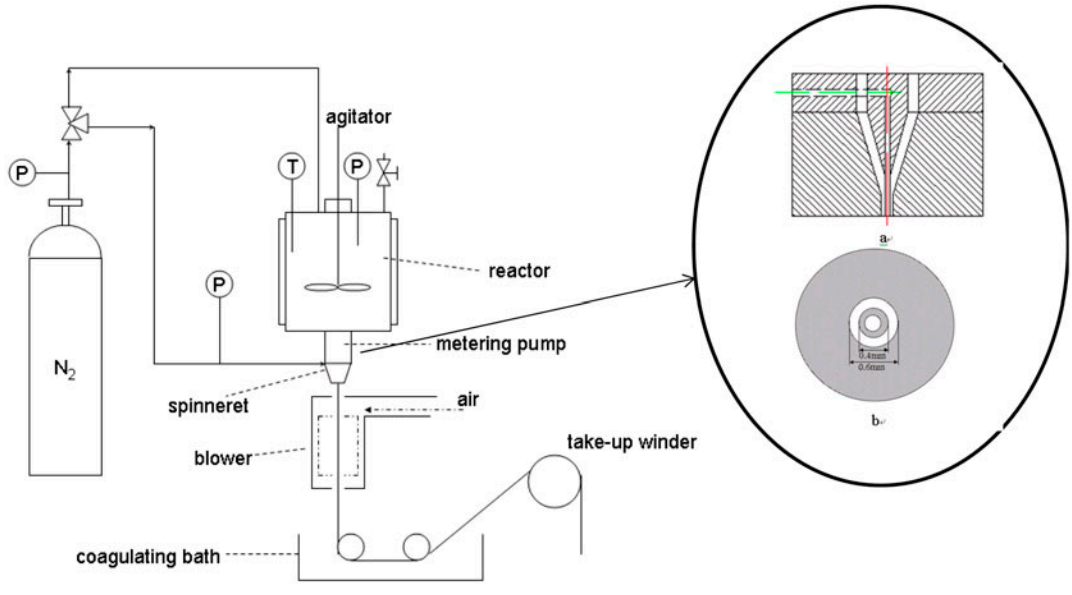

Fig. 2. The iPP hollow fiber membrane preparation process: (a) the structure of longitudinal section of the spinneret and (b) the structure of cross section of the spinneret.

2.3.5. LEPw measurement

The LEPw value was obtained using the method described by Smolders and Franken [30]. Firstly, a sample membrane was placed in a vessel that was filled with water. Then, the vessel pressure increased with compressed nitrogen. The pressure increased 10 kPa every time and kept constant for 5 min. When the pressure decreased at first time, the pressure was the liquid entry pressure. Every experiment was conducted twice and the final LEPw was the average value of experiment data. LEPw was measured for the maximum experimental pressure at which the membrane was not wetted by liquid.

LEPw was calculated by the Young–Laplace equation [31]:

$$\mathrm{LEP} = \frac{-2\gamma\cos\theta}{r_{\max}} \quad (1)$$

where γ is the surface tension of iPP, θ is the contact angle of water on the membrane, $r_{\max}$ is the maximum pore radius of membrane.

2.4. AGMD test

2.4.1. Membrane module parameters

Table 1 showed the characteristics of the three different membrane modules prepared for AGMD. The length, width, and height of the membrane module were 0.12, 0.08, and 0.8 m, respectively. The space between the hollow fiber membranes and the heat exchange tubes was 0.5 mm. They were used to investigate the effect of membrane thickness and T_1 on J_D, GOR and the TE during AGMD process. Fig. 1 was the schematic diagram of membrane module. The hollow fiber tubes and hollow fiber membranes which were potted together by an epoxy plug were arranged layer by layer. A PP net was placed between each layer of membranes and tubes to fix the air gap distance.

2.4.2. Experimental apparatus

The experimental apparatus was schematically shown in Fig. 3. The two brine feeds in AGMD process were pumped in a counter-current flow configuration. The cold brine feed was prepared in the thermostat *A*, and pumped into the bottom of hollow fiber tubes by a magnetic centrifugal pump. The cold feed flow rate was adjusted at 15L/h by a rotameter. The inlet temperature of the cold feed was maintained constant at 20, 25, 30, 35, 45, and 50℃, respectively. After flowing out from the top of the heat exchange hollow fiber tubes, the high saline water was flowed into the thermostat *B* and heated to 95℃. Our previous works [23–26] said that the permeate flux (J_D) increased as T_3 increased. In order to obtain higher permeate flux, the hot inlet feed temperature (T_3) was constant at 95℃ which was the highest temperature during our previous experiments. The hot feed was then pumped into the top of the porous membranes with an equal flow rate (15L/h) of the cold feed. The inlet and outlet temperature of the two brine feeds was determined with thermometers Pt100 with accuracy of ±0.1℃. In order to prevent the heat transfer between the MD system and the surrounding, heat preservation cottons were wrapped around the MD system tightly for several layers. When the whole system steadily operated, the permeate water was collected with a volumetric cylinder at the bottom of the membrane module and weighed every 10 min. The conductivity of the condense water was measured with a conductivity meter (DDSJ-308A, Shanghai Leici

Table 1
Details of the modules used for AGMD experiments

Membrane no.	Number of hollow fiber membrane	Number of hollow fiber tube	Modules length (m)	Effective surface area of hollow fiber membrane (m^2)
M-1	200	400	0.8	0.17
M-2	200	400	0.8	0.20
M-3	200	400	0.8	0.25

Membrane mode	ID/OD of hollow fiber tube (m)	The thickness of air gap (mm)	Packing density
M-1	0.4/0.5	0.5	0.2
M-2	0.4/0.5	0.5	0.2
M-3	0.4/0.5	0.5	0.2

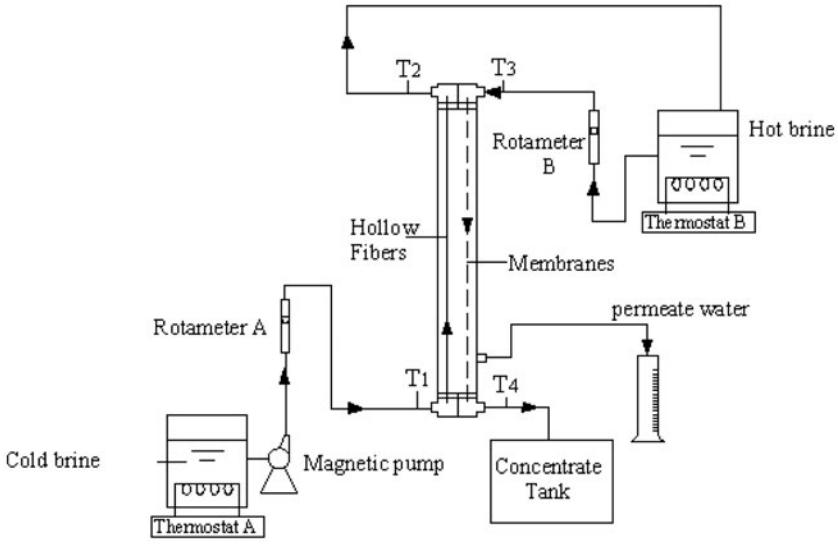

Fig. 3. Schematic diagram of the AGMD experimental apparatus.

Instrument Factory, Shanghai, China). Every experiment was repeated three times under the same operational condition, and the average value was calculated.

2.4.3. Performance indicators

The main performance parameters of the AGMD process are J_D, GOR, and the TE.

J_D was calculated as follow:

$$J_D = \frac{W_D}{S \cdot t} \tag{2}$$

where W_D was the weight of the permeate water within the time of t. S was the effective evaporation surface area based on the inner diameter of the hollow fiber membrane.

GOR was determined as below:

$$\mathrm{GOR} = \frac{W_D \cdot \Delta H}{Q_{in}} = \frac{W_D \cdot \Delta H}{W_h \cdot C_p(T_3 - T_2)} \tag{3}$$

where ΔH was the condensation latent heat of water vapor. Q_{in} was the heat input from the external heat thermostat B, W_h was the flow rate of hot brine feed, C_p was the specific heat capacity of hot brine feed, T_2 and T_3 were the temperatures of the outlet of cold brine feed and the inlet of hot brine feed, respectively.

The TE was obtained as follow:

$$\mathrm{TE} = \frac{Q_v}{Q_{all}} = \frac{W_D \cdot \Delta H}{W_c C_p(T_2 - T_1)} \tag{4}$$

where Q_{all} was the total heat transferred into the cold brine feed, and Q_v was the heat transferred for the evaporation of water, W_c was the flow rate of the cold brine feed, T_1 and T_2 were the temperatures of the inlet and outlet of the cold brine feed, respectively.

3. Results and discussion

3.1. Characterization of iPP hollow fiber membrane

There are two types of phase separation in the membrane preparation process using TIPS method: liquid–liquid phase separation and solid–liquid phase separation. During the cooling process, there is a competition between liquid–liquid phase separation and solid–liquid phase separation. If the liquid–liquid phase separation occupies the predominant position, it can form cellular or bicontinuous membrane structure. If the solid–liquid phase separation happens prior to liquid–liquid phase separation, it can form spherulitic or particulate structure [29].

The SEM morphologies of the three different iPP hollow fiber membranes were shown in Fig. 4. As shown in the cross section image, the membranes had bicontinuous structure indicating that L–L phase separation occurred first. What's more, the bicontinuous

structure was suitable for MD. Because the bicontinuous or cellular structure was the open pore structure and the pores were connective which was conducive to water vapor across the membrane during AGMD [32]. Membrane characteristics were listed in Table 2. From Table 2, we could see that the water flux slowly decreased with increase in the membrane thickness which was in agreement with the increase in membrane mass resistance as the membrane thickness increased. The membrane with large mean pore size and high porosity could improve the performance of MD module. The effect of pore size had been studied in our previous work [33]. High porosity not only could increase the thermal resistance which would increase TE, but also could improve the permeability of membrane [4]. The porosity and pore diameters could be assumed to be constant for small variation in order to investigate the influence of membrane thickness [21].

From Table 2, we could also see that tensile break strength of the three membranes were almost the same with the same ratio of membrane thickness to inner diameter. The tensile break strength was small when the membrane was thin. The tensile break strength was big if the membrane inner diameter was small. So the tensile break strength was nearly the same when the membrane thickness to inner diameter ratio was the same.

3.2. The performance of iPP hollow fiber membrane in AGMD process

The effect of T_1 and membrane thickness on the performance of membrane module was investigated, respectively. The membrane thickness of M-1, M-2, and M-3 was 67.2, 80.8, and 100.3 μm, respectively. The AGMD process was carried out with T_3 at 95˚C. T_1 varied from 25 to 50˚C with an interval of 5˚C. The sodium chloride concentration of brine feed was 6 wt% and the brine feed flow rate was 15 L/h.

3.2.1. Permeate water flux (J_D)

From Fig. 5, it was observed that J_D decreased with the increase in T_1. The driving force of MD was the vapor pressure difference due to brine temperature gradient across the hollow fiber microstructure membrane. When T_1 increased, the brine temperature gradient across the hollow fiber membrane decreased. The vapor pressure difference across the hollow fiber membrane decreased at the same time. The driving force of AGMD process decreased resulting in J_D decreased. The conductivity of the distillate from iPP hollow fiber membrane was less than 10.0 μS/cm, which indicated that the salt rejection of hot brine feed achieved 99.9% for all the prepared hollow fiber membranes.

The resistance of thickness of the hollow fiber membrane was smaller than the air gap which was the main resistance of AGMD, but it was necessary to research. The influence of the membrane thickness on J_D was seen in Fig. 5. It depicted that J_D decreased as the thickness of hollow fiber membrane increased in the same ratio of thickness to inner diameter. When the thickness of hollow fiber membrane increased, the resistance of water vapor molecular across the membrane increased. The number of water vapor molecular across the membrane decreased.

The maximum J_D could reach 6.62 kg/(m^2 h) at the thickness of membrane was 67.2 μm under T_1 = 25˚C, T_3 = 95˚C, and flow rate of 15L/h.

3.2.2. Gained output ratio

As shown in Fig. 6, GOR increased as T_1 increased. GOR was the function of (T_3–T_2) and J_D. GOR had proportional to J_D and an inverse correlation with (T_3–T_2). When T_1 increased, T_2 increased. Although J_D and (T_3–T_2) decreased as T_1 increased, (T_3–T_2) decreased faster than J_D which led to an increase in GOR. Fig. 6 also depicted that GOR decreased as the thickness of hollow fiber membrane increased in the same thickness to inner diameter ratio. J_D decreased as the thickness increased. The latent heat was less because J_D decreased. The less the latent heat was, the lower T_2 was. As a consequence of increasing membrane thickness, J_D decreased and (T_3–T_2) increased. So GOR decreased as membrane thickness increased.

The maximum GOR could reach 6.95 at the thickness of 67.2 μm under T_1 = 50˚C, T_3 = 95˚C, and flow rate of 15 L/h since the latent heat was recovered by the cold brine feed in heat exchange hollow fiber tubes. The GOR in DCMD process and in traditional AGMD process [34–38] were 0.1–0.65 and 0.7–0.98, respectively.

3.2.3. The TE

During MD process, the transmembrane heat transport could mainly be divided into two parts which were the latent heat used for evaporating the water and the heat conduction across the membrane. The TE in AGMD process was presented in Fig. 7. It illustrated that the TE varied from 78.81 to 89.42% and increased with the increase in T_1. Both J_D and (T_2–T_1) decreased as T_1 increased. When T_1 increased from 30

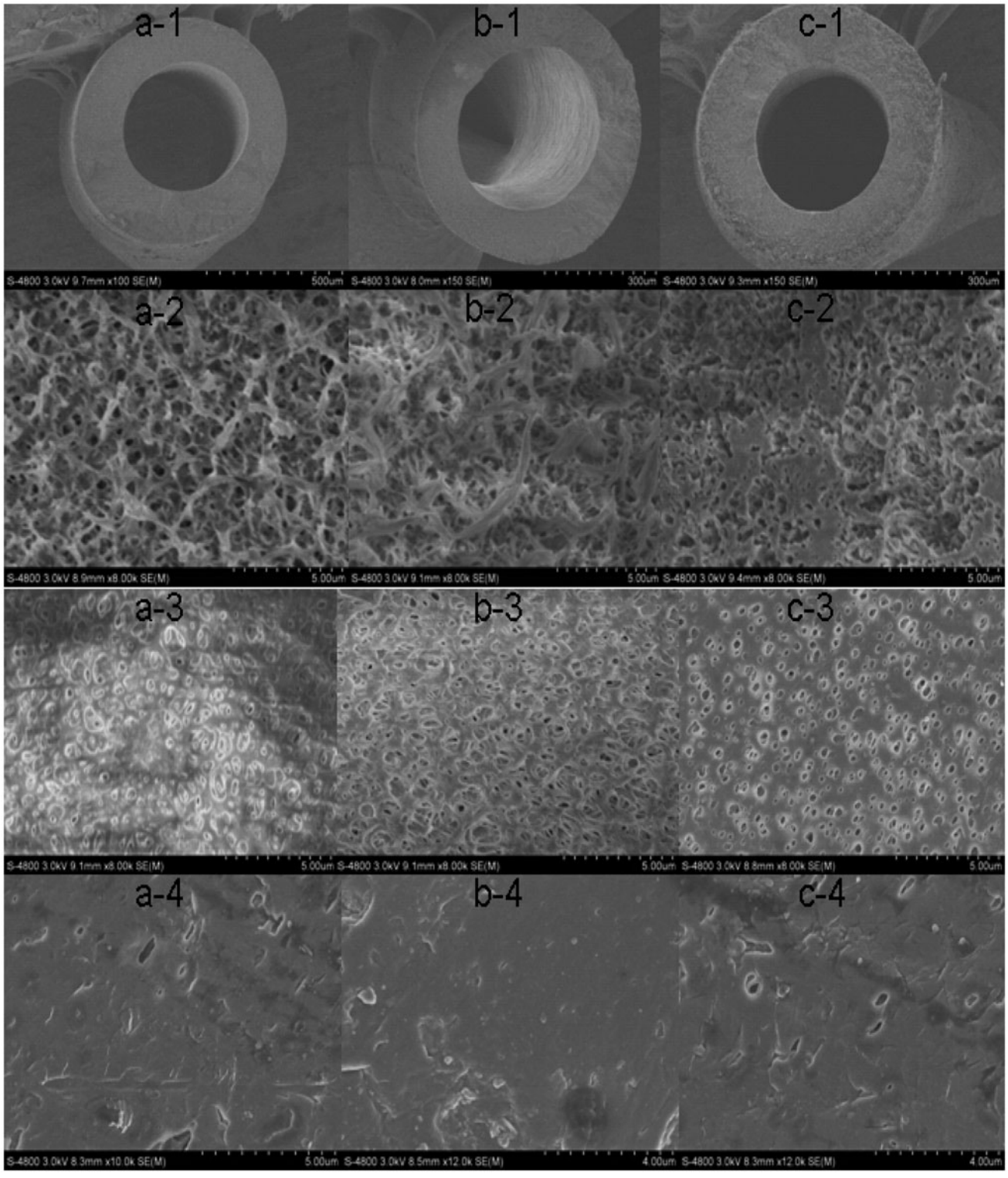

Fig. 4. SEM images of the iPP hollow fiber membranes: (a) the thickness is 67.2 μm; (b) the thickness is 80.8 μm; (c) the thickness is 100.3 μm; (1) is the full cross section; (2) is the cross section; (3) is the inner surface; (4) is the outer surface.

Table 2
Characteristic of the iPP hollow fiber membrane

Membrane no.	Thickness (μm)	ID/OD[a] (μm)	Thickness to inner diameter ratio	Water flux (L/m^2 h)	LEPw (MPa)
M-1	67.2 ± 3.5	342.4/476.8	0.2	1,920 ± 4	0.263 ± 0.00252
M-2	80.8 ± 5.3	401.1/562.7	0.2	1,860 ± 2	0.263 ± 0.00252
M-3	100.3 ± 2.6	499.6/700.2	0.2	1,810 ± 2	0.263 ± 0.00252
Membrane mode	Porosity (%)	Average pore size (μm)	Contact angle (°)	Tensile break strength (N)	
M-1	73.11 ± 0.22	0.25	101.87 ± 7.42	2.13 ± 0.24	
M-2	69.50 ± 1.03	0.23	101.87 ± 7.42	2.19 ± 0.16	
M-3	67.80 ± 0.46	0.22	101.87 ± 7.42	2.41 ± 0.19	

[a]ID/OD is the inner diameter/outer diameter.

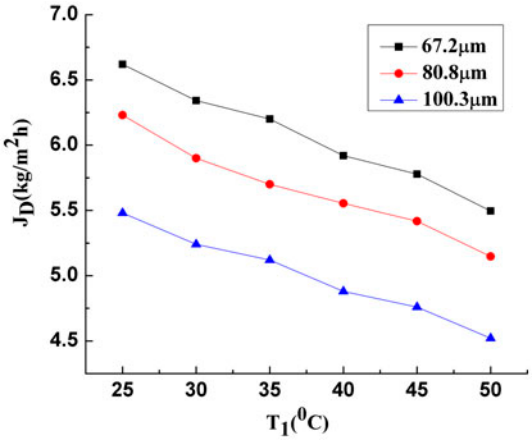

Fig. 5. Effect of inlet temperature of cold brine feed (T_1) and the thickness of membranes on J_D under T_3 = 95°C, F = 15 L/h and c = 60 g/L.

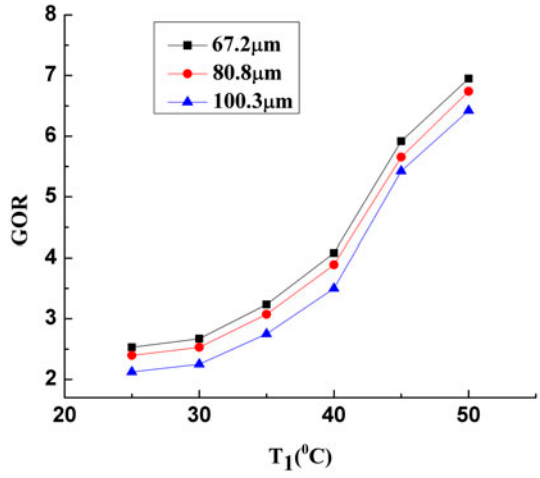

Fig. 6. Effect of inlet temperature of cold brine feed (T_1) and the thickness of membranes on GOR under T_3 = 95°C, F = 15 L/h, and c = 60 g/L.

to 35°C at T_3 = 95°C, (T_2–T_1) decreased by 4.2% from 49.5 to 47.4°C and J_D decreased by 2.2% from 6.34 to 6.20 kg/m^2 h. (T_2–T_1) decreased faster than J_D which led to an increase in the TE. Fig. 7 also showed that the TE increased as the thickness of hollow fiber membrane increased with the same thickness to inner diameter ratio. Because the heat transfer resistance across the membrane increased as membrane thickened, and heat loss became smaller.

The maximum TE was much higher than that of traditional MD modules. The TE in counter current DCMD was around 60–70% [39]. Yao et al. [34] obtained higher TE of 80% in continuous-effect MD module. Because the latent heat was recycled to preheat the cold brine feed when the water vapor condensed on the surface of the hollow fiber tubes. The heat provided from outside decreased and the TE increased. What's more, the contact of membranes and hollow fiber tubes led to heat loss because of heat conduction, the PP net in the AGMD module fixed the location of membranes and tubes and the air gap was constant.

Membrane thickness played an important role in MD process. J_D was inversely proportional to membrane thickness, however, the TE increased as membrane thickened. When the membrane was thicker, the mass transfer resistance of membrane was higher and J_D got lower. On the other hand, if the membrane was too thin, the heat conduction across the membrane would enhance which was not conductive to the operation of MD [40]. From our experiments, the suitable thickness of membrane was within the range of 70–90 μm.

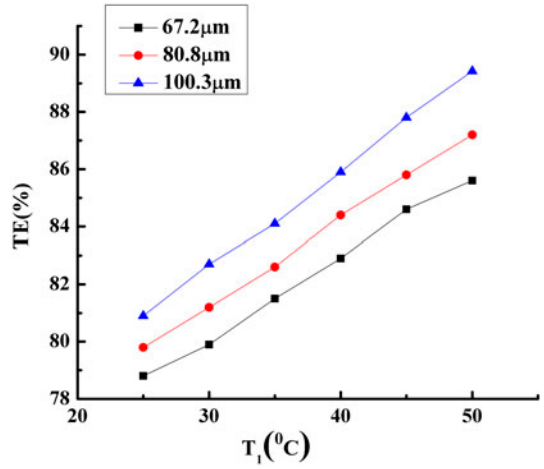

Fig. 7. Effect of inlet temperature of cold brine feed (T_1) and the thickness of membranes on TE under T_3 = 95°C, F = 15 L/h, and c = 60 g/L.

4. Conclusion

In the present work, the iPP hollow fiber membranes which had three different thicknesses (67.2, 80.8, and 100.3 μm) were prepared for AGMD through TIPS method using DOP and DBP as composite diluents. The morphology, PWF, porosity, tensile break strength and pore size of the prepared membrane were characterized. The AGMD module for desalination with internal latent heat recovery was set up. J_D, GOR, and the TE in AGMD were determined. The following conclusions were drawn:

(1) J_D decreased with the increase in T_1 and decreased as the membrane thickness increased with the same thickness to inner diameter ratio. The maximum J_D could reach 6.62 kg/(m^2 h) at the thickness of membrane 67.2 μm under T_1 = 5°C, T_3 = 95°C and flow rate of 15 L/h.
(2) GOR increased as T_1 increased and decreased as the membrane thickness increased. The maximum GOR could reach 6.95 at the thickness of membrane 67.2 μm under T_1 = 50°C, T_3 = 95°C, and flow rate of 15 L/h.
(3) The TE increased with the increase in T_1, and the maximum TE 89.42% was achieved with the membrane thickness 100.3 μm because latent heat recovery was to preheat cold brine feed and the decrease in heat loss resulted from the PP net.

Nomenclature

c	—	feed concentration (g/L)
F	—	volume flow rate (L/h)
GOR	—	gained output ratio
ΔH	—	water enthalpy (J/kg)
J_D	—	permeate water flux (kg/(m^{2}h))
S	—	area of membrane (m^2)
t	—	time (s)
TE	—	thermal efficiency
T_1	—	inlet temperature of cold brine feed (°C)
T_2	—	outlet temperature of cold brine feed (°C)
T_3	—	inlet temperature of hot brine feed (°C)
T_4	—	outlet temperature of hot brine feed (°C)
ε	—	the membrane porosity

References

[1] S. Devi, P. Ray, K. Singh, P.S. Singh, Preparation and characterization of highly micro-porous PVDF membranes for desalination of saline water through vacuum membrane distillation, Desalination 346 (2014) 9–18.
[2] D.Y. Hou, J. Wang, X.C. Sun, Z.G. Ji, Z.K. Luan, Preparation and properties of PVDF composite hollow fiber membranes for desalination through direct contact membrane distillation, J. Membr. Sci. 405–406 (2012) 185–200.
[3] M. Qtaishat, M. Khayet, T. Matsuura, Guidelines for preparation of higher flux hydrophobic/hydrophilic composite membranes for membrane distillation, J. Membr. Sci. 329 (2009) 193–200.
[4] M.S. El-Bourawi, Z.W. Ding, R.Y. Ma, M. Khayet, A framework for better understanding membrane distillation separation process, J. Membr. Sci. 285 (2006) 4–29.
[5] D.Y. Hou, G.H. Dai, H. Fan, J. Wang, C.W. Zhao, H.J. Huang, Effects of calcium carbonate nano-particles on the properties of PVDF/nonwoven fabric flat-sheet composite membranes for direct contact membrane distillation, Desalination 347 (2014) 25–33.
[6] D. Singh, K.K. Sirkar, High temperature direct contact membrane distillation based desalination using PTFE hollow fibers, Chem. Eng. Sci. 116 (2014) 824–833.
[7] S. Gunko, S. Verbych, M. Bryk, N. Hilal, Concentration of apple juice using direct contact membrane distillation, Desalination 190(1–3) (2006) 117–124.
[8] J. Walton, H. Lu, C. Turner, S. Solis, H. Hein, Solar and Waste Heat Desalination by Membrane Distillation, College of Engineering University of Texas, EI Paso, 2004.
[9] S. Bandini, C. Gostoli, G.C. Sarti, Separation efficiency in vacuum membrane distillation, J. Membr. Sci. 73(2–3) (1992) 217–229.
[10] D. Singh, K.K. Sirkar, Desalination of brine and produced water by direct contact membrane distillation at high temperatures and pressures, J. Membr. Sci. 389 (2012) 380–388.

[11] D.Y. Hou, J. Wang, X.C. Sun, Z.K. Luan, C.W. Zhao, X.J. Ren, Boron removal from aqueous solution by direct contact membrane distillation, J. Hazard. Mater. 177 (2010) 613–619.
[12] J. Phattaranawik, R. Jiraratananon, A.G. Fane, Effect of pore size distribution and air flux on mass transport in direct contact membrane distillation, J. Membr. Sci. 215 (2003) 75–85.
[13] M. Gryta, Influence of polypropylene membrane surface porosity on the performance of membrane distillation process, J. Membr. Sci. 287 (2007) 67–78.
[14] F.A.A. Al-Rub, F. Banat, K. Beni-Melhim, Parametric sensitivity analysis of direct contace membrane distillation, Sep. Sci. Technol. 37 (2002) 3245–3271.
[15] M. Gryta, M. Tomaszewska, Heat transport in the membrane distillation process, J. Membr. Sci. 144 (1998) 211–222.
[16] A. Alkhudhiri, N. Darwish, N. Hilal, Membrane distillation: A comprehensive review, Desalination 287 (2012) 2–18.
[17] M. Khayet, Membranes and theoretical modeling of membrane distillation: A review, Adv. Colloid Interface Sci. 164 (2011) 56–88.
[18] K.W. Lawson, D.R. Lloyd, Membrane distillation, J. Membr. Sci. 124 (1997) 1–25.
[19] R.W. Schofield, A.G. Fane, C.J.D. Fell, Heat and mass transfer in membrane distillation, J. Membr. Sci. 33 (1987) 299–313.
[20] M. Khayet, M.P. Godino, J.I. Mengual, Possibility of nuclear desalination through various membrane distillation configurations: A comparative study, Int. J. Nucl. Desalin. 1(1) (2003) 30–46.
[21] F. Laganà, G. Barbieri, E. Drioli, Direct contact membrane distillation: Modelling and concentration experiments, J. Membr. Sci. 166 (2000) 1–11.
[22] R.W. Schofield, A.G. Fane, C.J.D. Fell, Gas and vapor transport through microporous membrane. I. Knudsen-Poiseuille transition, J. Membr. Sci. 53 (1990) 45–56.
[23] H.X. Geng, Q.F. He, H.Y. Wu, P.L. Li, C.Y. Zhang, H.Y. Chang, Experimental study of hollow fiber AGMD modules with energy recovery for high saline water desalination, Desalination 344 (2014) 55–63.
[24] H.X. Geng, H.Y. Wu, P.L. Li, Q.F. He, Study on a new air-gap membrane distillation module for desalination, Desalination 334 (2014) 29–38.
[25] H.X. Geng, J. Wang, C.Y. Zhang, P.L. Li, H.Y. Chang, High water recovery of RO brine using multi-stage air gap membrane distillation, Desalination 355 (2015) 178–185.
[26] Q.F. He, P.L. Li, H.X. Geng, C.Y. Zhang, J. Wang, H.Y. Chang, Modeling and optimization of air gap membrane distillation system for desalination, Desalination 354 (2014) 68–75.
[27] Z.S. Yang, P.L. Li, L.X. Xie, Z. Wang, S.C. Wang, Preparation of iPP hollow-fiber microporous membranes via thermally induced phase separation with co-solvents of DBP and DOP, Desalination 192 (2006) 168–181.
[28] Z.S. Yang, P.L. Li, H.Y. Chang, S.C. Wang, Effect of diluent on the morphology and performance of IPP hollow fiber microporous membrane via thermally induced phase separation, Chin. J. Chem. Eng. 14(3) (2006) 394–397.
[29] J. Yang, D.W. Li, Y.K. Lin, X.L. Wang, F. Tian, Z. Wang, Formation of a bicontinuous structure membrane of polyvinylidene fluoride in diphenyl ketone diluent via thermally induced phase separation, J. Appl. Polym. Sci. 110 (2008) 341–347.
[30] K. Smolders, A.C.M. Franken, Terminology for membrane distillation, Desalination 72 (1989) 249–262.
[31] E. Guillen-Burrieza, A. Servi, B.S. Lalia, H.A. Arafat, Membrane structure and surface morphology impact on the wetting of MD membranes, J. Membr. Sci. 483 (2015) 94–103.
[32] M.R.M. Abed, S.C. Kumbharkar, A.M. Groth, K. Li, PVDF hollow fiber membrane with interconnected bicontinuous structures produced via immersion precipitation technique, Procedia Eng. 44 (2012) 571–573.
[33] C.Y. Zhang, H.X. Geng, Q.C. Lang, L.P. Li, X.Y. Wu, Study on a new air gap membrane distillation module for desalination, CIESC J. 66 (2015) 4000–4006.
[34] K. Yao, Y.J. Qin, Y.J. Yuan, L.Q. Liu, F. He, Y. Wu, A continuous-effect membrane distillation process based on hollow fiber AGMD module with internal-heat recovery, AICHE J. 59 (2012) 1278–1297.
[35] F. He, J. Gilron, K.K. Sirkar, High water recovery in direct contact membrane distillation using a series of cascades, Desalination 323 (2013) 48–54.
[36] J. Gilron, L. Song, K.K. Sirkar, Design for cascade of crossflow direct contact membrane distillation, Ind. Eng. Chem. Res. 46 (2007) 2324–2334.
[37] S. Alobaidani, E. Curcio, F. Macedonio, G.D. Diprofio, H. Alhinai, E. Drioli, Potential of membrane distillation in seawater desalination: Thermal efficiency, sensitivity study and cost estimation, J. Membr. Sci. 323 (2008) 85–98.
[38] J.G. Lee, W.S. Kim, Numerical study on multi-stage vacuum membrane distillation with economic evaluation, Desalination 339 (2014) 54–67.
[39] D. Singh, K.K. Sirkar, Desalination by air gap membrane distillation using a two hollow-fiber-set membrane module, J. Membr. Sci. 421–422 (2012) 172–179.
[40] L. Yang, Z.W. Ding, R.Y. Ma, Study on temperature polarization in membrane distillation, Membr. Sci. Technol. 24(3) (2004) 4–9.